Int. J. Multiphase Flow Vol. 7, No. 6, pp. 677–701, 1981
Printed in Great Britain.

0301-9322/81/060677-25$02.00/0
Pergamon/Elsevier

CRITICAL HEAT FLUX PREDICTIONS DURING BLOWDOWN TRANSIENTS

J. C. M. LEUNG, K. A. GALLIVAN† and R. E. HENRY‡

Reactor Analysis and Safety Division, Argonne National Laboratory, Argonne, IL 60439, U.S.A.

and

S. G. BANKOFF

Department of Chemical Engineering, Northwestern University, Evanston, IL 60201, U.S.A.

(*Received* 22 *April* 1980; *in revised form* 20 *January* 1981)

Abstract—A best-estimate prediction of transient critical heat flux (CHF) is based on instantaneous local-conditions. Eight correlations were tested against most recent blowdown heat-transfer data obtained in the U.S. The prediction results are summarized in a table in which both CISE and Biasi round-tube correlations are found to be capable of predicting the early CHF that occurs after flow reversal in the order of 1 s.

The Griffith–Zuber correlation is credited for its prediction of the delay CHF that occurs in a quiescent state with slowly decaying mass velocity. A mass-velocity criterion is also suggested for its application. In many experiments, the early CHF can be closely correlated by the $X = 1.0$ criterion; this is certainly indicative of a dryout mechanism. As for the delay CHF, a pool-boiling-type hydrodynamic crisis is suggested.

1. INTRODUCTION

The onset of critical heat flux (CHF) during abnormal conditions and hypothetical accidents of an operating nuclear reactor is of utmost importance in the safety analysis and licensing calculation. The present study focused attention primarily on the pressurized water reactor (PWR) system since the associated loss-of-coolant accident (LOCA) would result in the most rapid and severe thermal-hydraulic transient, particularly for an inlet (cold-leg) pipe guillotine rupture. The time at which efficient cooling ceases at the fuel-rod surface is a major parameter in LOCA analyses because of its influence on the peak cladding temperature. The onset of such a phenomenon is widely referred to as a boiling crisis or CHF condition.

Earlier, Leung (1978) conducted a literature survey on transient CHF work and found many experimental investigations aimed at studying LOCAs. However, analyses of the CHF phenomena in these experiments have been very few. This present study intends to provide a more unified treatment of CHF prediction during blowdown with a wide range of flow and pressure conditions. An earlier paper (Leung & Gallivan 1980) presented similar treatment for flow-decay transients obtained in round-tube geometry.

2. PREDICTIONAL METHOD

The approach taken in the present study is to calculate the fluid behavior in the heated core, and to predict the onset of CHF using some well-known CHF correlations. To accomplish this task, a predictional method was developed with the following key features:

(1) Calculation of local fluid conditions.
(2) Boundary conditions being supplied from experimental measurements.
(3) Prediction of transient CHF based on "local-conditions" hypothesis.

A simple computer code named CODA (Coolant Dynamics Analysis), embodying the above features, has been developed to analyze the blowdown data. CODA is simply a one-dimensional code with homogeneous equilibrium flow formulation. Any explicit method that attempts to account for the acoustic (or pressurewave propagation) phenomena would require excessive

†Present address: Computer Science Dept., University of Illinois, Urbana, IL 61801, U.S.A.
‡Present address: Fauske & Associates, Willowbrook, IL 60521, U.S.A.

computation time since the numerical stability is dictated by the Courant's criterion,

$$\Delta t < \frac{\Delta z}{c + |u|} \qquad [1]$$

where Δt, Δz, c and u are time step, nodal spacing, sonic velocity, and particle velocity. For a nodal spacing of 5 cm and a typical sonic velocity of 1500 m/s in water, the allowable time step is less than 3.3×10^{-5} s. Since the acoustic phenomenon plays a major role only during the initial subcooled blowdown phase and at locations near the break, the present scheme neglects the acoustic phenomenon completely and assumes that density (ρ) can be evaluated adequately as a function of enthalpy (h) alone as first suggested by Meyers (1961). Essentially this assumption decouples the momentum equation from the continuity and energy equations since the feedback of pressure on density is ignored. Of course the underlying assumption is that the thermodynamic properties can be evaluated at the system pressure which is taken to be constant spatially throughout the region of interest. This is particularly valid for high pressure system such as PWRs because the pressure variation inside the reactor core is small in comparison with the system pressure, and the resulting change in thermodynamic properties is minimal.

By neglecting the kinetic energy term in the energy equation, the continuity and energy equations can be written as

$$A \frac{\partial \rho}{\partial t} + \frac{\partial}{\partial z} GA = 0 \qquad [2]$$

$$\frac{\partial h}{\partial t} + \frac{G}{\rho} \frac{\partial h}{\partial z} = \frac{\phi P_h}{\rho A} + \frac{1}{\rho} \frac{\mathrm{d}P}{\mathrm{d}t} \qquad [3]$$

where ϕ and P_h are respectively the channel heat flux and heated perimeter. Further manipulation of these two equations leads to an expression that describes the local rate of fluid expansion in single phase and voiding in two phase. The particular result in two phase for a constant-area flow channel is

$$\frac{\partial u}{\partial z} = \underbrace{\frac{\phi P_h v_{LG}}{A h_{LG}}}_{\text{a}} + \underbrace{\frac{v_{LG}}{h_{LG}} \left[1 - \frac{1}{v} \left(\frac{\partial h}{\partial P} \right)_x \right] \frac{\mathrm{d}P}{\mathrm{d}t}}_{\text{b}} \qquad [4]$$

where v is the specific volume, and subscript LG refers to the difference between liquid and vapor property. It can be seen that the volumetric flux variation of the two-phase mixture depends on the (a) wall heat flux and (b) flashing as a result of depressurization. The step-by-step solution is outlined by Leung (1980), but basically the finite-difference form of [2] and [3] was integrated in step-wise manner using a predictor-corrector (explicit) scheme together with the equation of state. For this scheme the numerical-stability criterion is relaxed to

$$\Delta t < \frac{\Delta z}{|u|} \qquad [5]$$

which implies that the time step be such that no fluid particle is allowed to traverse more than one nodal spacing.

In addition, the following boundary conditions are required:

(1) System pressure.
(2) Mass flow rate at either inlet or outlet.
(3) Fluid enthalpy at inflow boundary.
(4) Heat flux into coolant.

Pressure in the simulated reactor core is usually measured with a strain gauge transducer and this measurement is readily available for input as a boundary condition. Mass flow rate is typically measured with an instrumented spool spice which consists of a densitometer, a turbine flowmeter, and a drag disk. However, the mass flow calculation is not so straightforward, particularly in a highly transient two-phase flow situation; some of the difficulties will be examined in section 4.

At present, the third boundary condition is handled by simply treating the inflow enthalpy to be having the same value as the initial value; for example, after an initial flow reversal at the outlet of the core, the inflow enthalpy is taken to be at the initial outflow value.

The fourth boundary condition requires a transient heat conduction analysis inside the heater. Because of the heat capacity of the electric heater (or fuel rod) the surface heat flux lags the power during the transient and varies with the coolant conditions. In the case of heaters with embedded thermocouples, the determination of surface heat flux requires the so-called "inverse" heat conduction calculation. An existing code named HETRAP (Malang 1974) was employed for this calculation. The required input to this code are two temperature measurements (usually one near-wall and one centerline temperature) together with the power history. This calculation was performed prior to and independent of the CODA calculation.

At the present state of the art, CHF predictions during transients are the combined product of a thermal-hydraulic code providing the instantaneous local fluid conditions and some appropriate steady-state CHF correlations. The CHF correlations selected in the present study are listed in table 1 and include both round-tube and rod-bundle correlations. Round-tube correlations are included because two recent heat-transfer packages (TRAC-P1A 1979, Bjornard & Griffith 1978) suggested for analyzing PWR blowdown behavior use CHF correlations developed for internal flow inside round tubes. Furthermore, Leung (1980) has shown that for limited rod-bundle data, the CISE round-tube correlation demonstrated acceptable prediction. Many other rod-bundle correlations were developed for low quality or subcooled departure from nucleate boiling (DNB) type crisis and for very limited pressure range; hence these correlations were not employed in our study. The W-3 correlation (Tong 1977), which is still widely used for reactor-core design, was originally developed for quality less than 0.15 at or above 7.0 MPa. However at quality greater than 0.5 and pressures below 12 MPa, this correlation yielded negative CHF values. Therefore, it was unacceptable in our analysis. A detailed listing of these correlations is presented in the Appendix.

Table 1. CHF correlations used in CODA and their range of applicability

Correlations	Geometry	Pressure (MPa)	Mass Velocity (kg/m^2s)	Quality	Remarks
Bowring (1972)	Round tube	0.2-19	136-18600	all x	3792 data points
Biasi (1967)	Round tube	0.3-14	100-6000	∿0 to 1.0	4500 data points
CISE (Bertoletti 1965)	Round tube	4.5-15	∿100-4000	∿0 to 1.0	Been shown to predict Freon data
B&W-2 (Gellerstedt 1969)	Rod bundle	14-16.6	1017-5430	-0.03 to 0.20	Only DNB data
CONDIE (1978)	Rod bundle	3.0-17	70-4700	-0.1 to 1.0	Total of 5163 data points
GE (Slifer 1971)	Rod bundle	6.9	<680	0 to 0.84	Low-flow data
Hsu-Beckner (1977)	Rod bundle	6-15	All	∿0 to 1.0	From PWR & BWR blowdown data
Griffith-Zuber (1977)	Short annulus	All range	Low G	0 to 1.0	Countercurrent and low flow

3. EXPERIMENTAL DATA

The present data base includes loss-of-coolant experiments conducted at major U.S. facilities such as the Columbia University heat-transfer loop, the Power Burst Facility (PBF), the Thermal Hydraulic Test Facility (THTF), the Semiscale Mod-1, and Mod-3 facilities. Because of time limitation, only selected experiments from these facilities were used in the present study as listed in table 2. Nearly all of these experiments were intended to simulate PWR LOCA with double-ended cold-leg breaks. Their initial conditions are summarized in the table also. CHF occurred as early as 0.4 s immediately following flow reversal, and as late as 25 s, while one of these tests exhibited no CHF at all. This wide range of times indeed deserves a careful and accurate prediction.

4. RESULTS AND DISSCUSSIONS

4.1 *Local fluid conditions calculations*

Using the "local-conditions" hypothesis, CHF prediction is dependent on the local fluid conditions such as pressure, mass velocity, and quality. Therefore, before the CHF prediction results are presented, a discussion of the problems associated with the local fluid condition calculation is in order here.

Among the input boundary conditions for the present calculation, the one that exerts the greatest uncertainty is the mass-velocity boundary specification. In these blowdown experiments, mass flow rate is usually measured with an instrumented spool piece which consists of: (i) a densitometer measuring density ρ, (ii) a turbine meter measuring volumetric flow Q, and (iii) a drag disk measuring momentum flux ρu^2. However, keep in mind that these quantities being measured are only approximately correct in two-phase flow situation as discussed by Silverman (1977). In evaluating the mass flow rate, a typical assumption is that the flow properties are uniform over the cross section. In addition, the homogeneous flow (equal velocity) assumption is employed to evaluate mass flow rate W in the following ways:

Method 1 $W_1 = \rho Q$

Method 2 $W_2 = A\sqrt{(\rho(\rho u^2))}$

Method 3 $W_3 = \dfrac{A(\rho u^2)}{Q/A}$.

Here method 1 uses the combination of densitometer and flow meter data, whereas method 2 use the densitometer and drag-disk data. Method 3 is seldom used since it does not utilize the densitometer data which are usually more reliable than the other two. Experimentally the turbine meter was found to respond much slower than the drag disk, particularly in a flow-reversal situation. For example, in the Loss-of-Fluid Test (LOFT) facility, the 10–90 percent rise time for the turbine and the drag disk was reported by Silverman to be about 50 and 5 ms, respectively.

Although the drag-disk transducer is more capable of following the rapid flow-reversal situation, it often showed other signs of difficulty such as a calibration drift. This can be inferred from Semiscale Mod-1 Test S-28-1 (Collins *et al.* 1977) during single-phase flow prior to blowdown; the turbine-meter flow rate (W_1) and the drag-disk flow rate (W_2) at the core inlet were 6.80 and 3.66 kg/s, respectively. The turbine-meter flow rate was felt to be correct because it agreed with other redundant measurements in the loop. Furthermore, it yielded a satisfactory overall heat balance inside the core. Davis (1978) postulated a systematic error for the drag-disk data, and suggested the momentum flux be adjusted by a constant multiplier C^2 in order to bring agreement between the two mass flow rates W_1 and W_2. This correction factor was given as the ratio of the steady-state mass flow,

$$C = \frac{W_1}{W_2}. \qquad [6]$$

The resulting drag-disk flow rate is compared with the turbine-meter flowrate in figure 1.

Table 2. Initial conditions of loss-of-coolant experiments

Facility	Test	Reference	Pressure MPa	Inlet Temperature °C	Mass Flowrate kg/s	Core Power MW	Remarks
CE/EPRI 5 × 5 rod bundle axial uniform flux 3.81 m	BHT-25	Hsia (1977)	13.7	296	9.3	1.77	Inlet break; no CHF
LOFT Columbia loop 5 × 5 bundle axial uniform flux 1.68 m	2-5 & 2-12	Gottula (1978)	15.2	257	4.2	1.42	Double-ended
PBF 4 shrouded fuel rods chopped-cosine 0.91 m	LOC-11C	Buckland (1978)	15.3	323	2.63	0.18	Double-ended; delay CHF
THTF bundle #1 7 × 7 chopped-cosine 3.66 m	105	Clemons (1977)	15.5	285	19.9	6.0	40% inlet-60% outlet
	104	Leon (1978)	15.5	287	20.0	6.0	50% inlet-50% outlet
	178	Craddick (1979)	15.9	277	19.6	3.7	32% inlet-28% outlet
	181	Craddick (1979)	14.2	267	13.4	1.7	20% inlet
	177	Craddick (1980)	15.4	276	21.0	3.7	32% inlet-28% outlet
Semiscale Mod-1 40 rod bundle chopped-cosine 1.68 m	S-02-1	Crapo (1975)	15.6	286	7.8	1.2	DEHL;[a] delay CHF
	S-02-9	Crapo (1976)	15.5	283	7.4	1.56	DECL[b]
	S-29-2	Crapo (1976)	12.2	283	7.4	1.58	DECL; reduced pressure
	S-28-1	Collins (1977)	15.8	284	6.8	1.4	DECL; early and delay CHF
	S-06-6	Esparza (1977)	15.8	290	4.9	1.0	DECL; mostly delay CHF
Semiscale Mod-3 5 × 5 bundle chopped-cosine 3.66 m	S-07-3	Gillins (1978)	15.9	285	9.5	2.05	DECL
	S-07-9	Miyasaki (1979)	16.1	284	8.6	2.0	DECL

[a] DEHL = double-ended hot leg break.

[b] DECL = double-ended cold leg break.

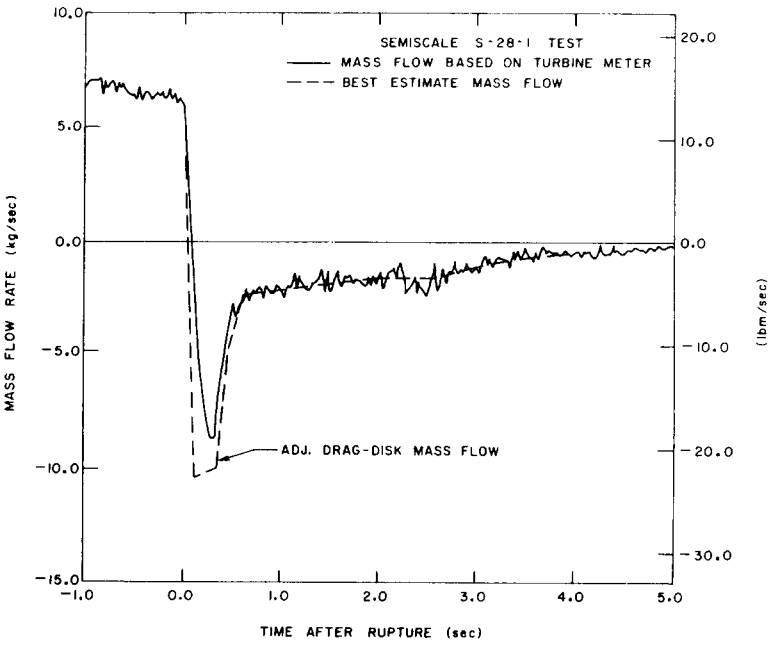

Figure 1. Core inlet mass flowrate during Semiscale Test S-28-1.

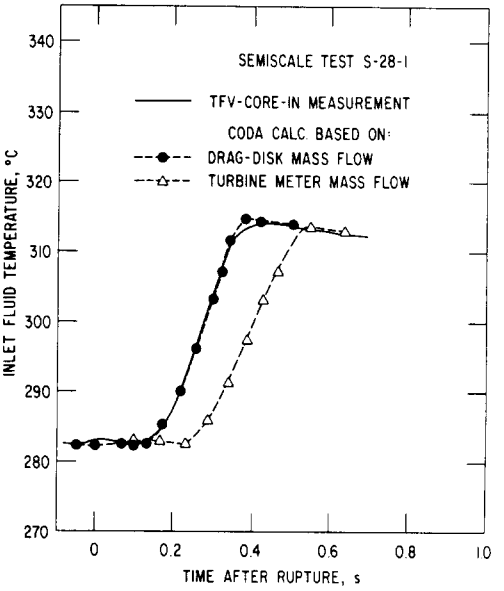

Figure 2. Core inlet temperature prediction.

The success of using the adjusted drag-disk data is demonstrated in figure 2, where the CODA- calculated core-inlet temperature and the thermocouple measurement are compared. The excellent prediction in the fluid temperature using the adjusted mass flow reflects a best-estimate thermal-hydraulic calculation during the early blowdown phase. Since the liquid was still subcooled during the first 400 ms at the core inlet, the fluid temperature is a direct measurement of the enthalpy which is calculated to rise rapidly as a result of flow reversal. Indeed, using the turbine-meter mass flow in this early period results in a much slower response in temperature rise which is far from acceptable as shown in the figure.

Similar treatment of the drag-disk measurement was performed for Semiscale Mod-1 Test S-02-9 (Crapo *et al.* 1976) although the correction factor in this case was much closer to unity. The calculated density is compared to the experimental data in figure 3 with favorable results.

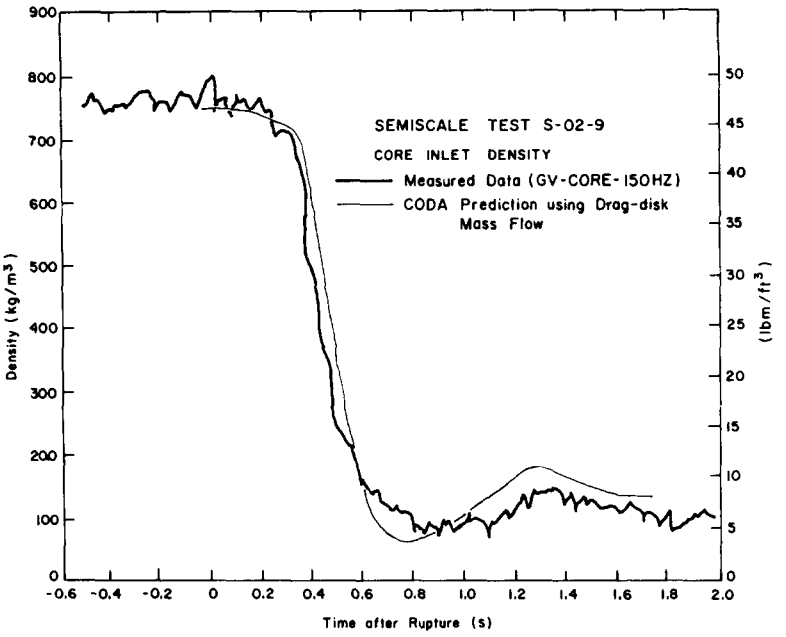

Figure 3. Core inlet density prediction.

In the Semiscale Mod-3 facility, a full-length 5×5 PWR bundle was accommodated with in-core measurements consisting of numerous densitometers and a drag-screen (here a screen target is employed) device at the bottom of the heated core. For Test S-07-3 (Gillins *et al.* 1978) the drag-screen measurement has to be adjusted in a similar fashion to yield identical mass flow as sensed by turbine meters in the downcomer and upper-plenum locations during steady-state operation. The resulting mass-flow data, as shown in figure 4, exhibit good agreement with the turbine-meter mass flow measured in the external downcomer during the first 0.5 s (the turbine flow-meter demonstrated much improved response than the one employed in the Mod-1 facility). This result, therefore, justifies the correction procedure since during this period the liquid was still subcooled in the lower core region, and from the continuity equation, [2], the temporal change of density ($\partial\rho/\partial t$) is necessarily small in the liquid regime, implying that the

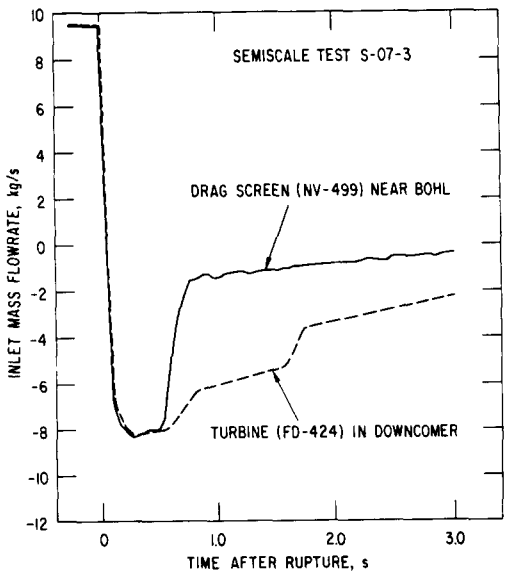

Figure 4. Comparison of mass flow measurements at core inlet and external downcomer.

mass flow rate is nearly constant spatially. This no longer holds, of course, when the two-phase mixture arrived at the lower core as illustrated in the figure at about 0.6 s.

Using the adjusted drag-screen flow rate as an input, the mass velocities at three levels in the heated core as calculated by CODA are shown in figure 5. A bidirectional flow configuration prevailed early in the blowdown as flow was leaving via both the top and bottom of the heated core. A complete flow reversal was calculated in the upper core at 0.7 s. This reversal brought about an increase in density since lower enthalpy fluid in the upper plenum began to reach the upper core. This flow behavior appears to be supported by the local density measurement as shown in figure 6. Finally, the predicted and calculated density at the core inlet is compared in figure 7 where generally good agreement is obtained.

In summary, encouraging results have been obtained for local fluid conditions calculations using CODA as demonstrated by the good agreement with in-core measurements. In the cases

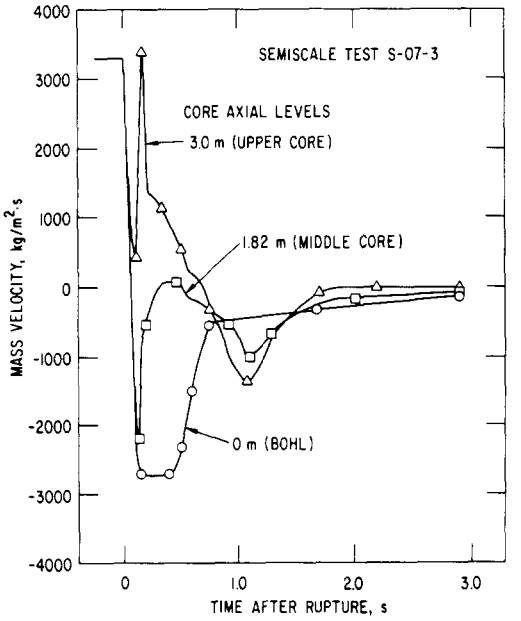

Figure 5. Calculated mass velocity behavior inside heated core.

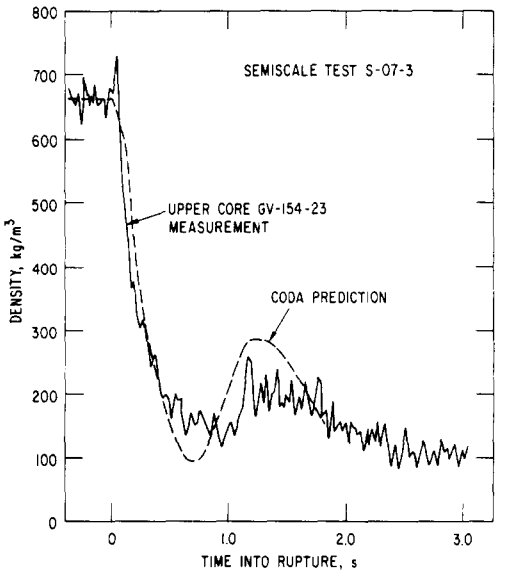

Figure 6. Comparison of predicted upper core density with data.

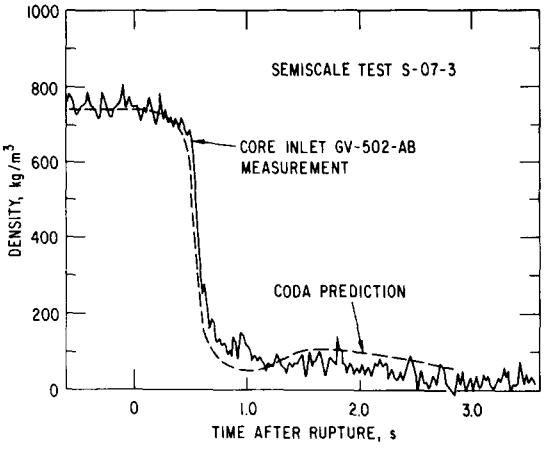

Figure 7. Core inlet density prediction.

presented here, the drag-disk (or screen) data required adjustment and the correction procedure seems to be justified.

4.2 *Transient CHF prediction using "local-conditions" hypothesis*

The CHF data and prediction results are presented in the form of plots of axial elevation vs time. The conventional critical-heat-flux ratio (CHFR) was calculated by CODA at various locations for each correlations. CHFR is a measure of the margin to CHF and is defined as

$$\text{CHFR} = \frac{\text{Critical heat flux}}{\text{Local heat flux}}. \qquad [7]$$

Hence, a CHFR value of less than 1.0 implies that CHF has been exceeded. In subsequent figures, the loci of CHFR = 1.0 are plotted; an example is given in figure 8. The leading edge of the curve of CHFR = 1.0 therefore represents the predicted CHF onset, but the trailing edge does not necessarily imply rewet or return to nucleate boiling. The reason for this is that other factors such as surface temperature and surface properties also play a major role in determining the rewet phenomena. Furthermore, when the surface heat flux is estimated by an inverse heat-conduction technique, the actual onset of CHF results in a much reduced heat flux which

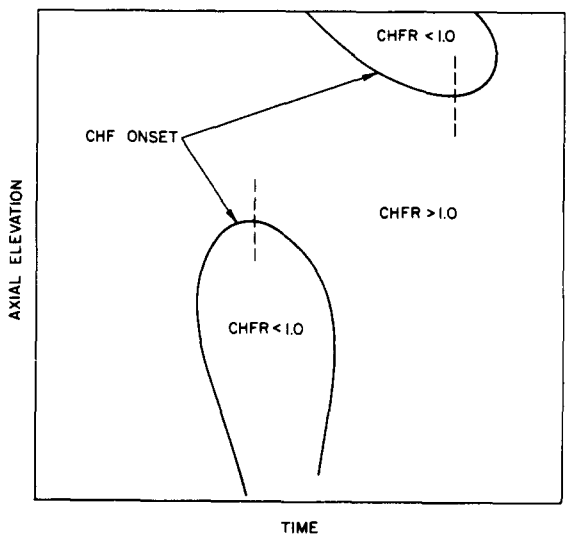

Figure 8. Example of CHF prediction plot.

can sometimes cause the CHFR to go above one. Since rewet is beyond the scope of the present study, the trailing edge in most cases was left out except when later CHF was predicted.

Due to space limitation only the highlights of some representative predictions are presented below.

LOFT—Columbia loop blowdown tests 2–5 *and* 2–12. Figure 9 shows the first indication of the thermal excursions at various levels of the 5×5 bundle. To properly determine the time to CHF, the response time of each thermocouple has to be taken into account by the equation

$$t_{CHF} = t_{TC} - \tau_{TC} \quad [8]$$

where t_{TC} = time of the first indication of temperature rise and τ_{TC} = overall response time of individual thermocouple and was determined experimentally at zero flow. Figure 9 shows the average t_{CHF} at each level together with the standard deviation (S.D.) After the response time is accounted for, CHF is seen to occur rather uniformly throughout the entire bundle. The result of CODA's prediction is summarized in figures 10 and 11. All three round-tube CHF correlations (CISE, Biasi and Bowring) exhibit close prediction of t_{CHF}. Both Hsu–Beckner and Condie correlations underpredict the time, whereas GE and B&W–2 correlations yield good agreement. Indeed, complete evaporation of liquid was calculated to occur rather uniformly over the entire core during 0.9–1.0 s, as indicated by the calculated line for $x = 1.0$ in figure 11. Hence the dryout mechanism was responsible for the CHF onset.

Semiscale Mod–1 blowdown tests. In Semiscale Test S–02–9 (cold-leg break), CHF was detected in the lower half of the core between 0.6 and 0.7 s with most of them exhibiting rewet behavior above the 0.76–m elevation. The CHF predictions by various correlations are shown in figures 12–14. Biasi, CISE and B&W–2 correlations are seen to predict the data well, while GE, Condie, Hsu–Beckner and Griffith–Zuber correlations tend to underpredict the time. The present finding, however, differed somewhat from Snider's (1977) conclusion in which the best prediction was obtained using GE correlation while Biasi and B&W–2 were found to be adequate.

Semiscale Test S–02–1 is one of the very few hot-leg break tests available for analysis. This

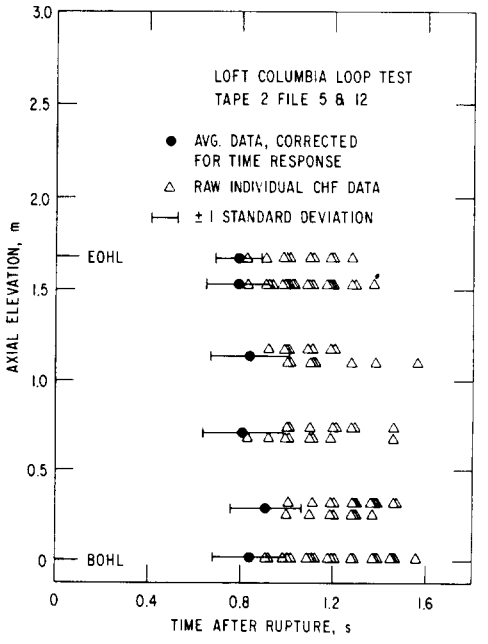

Figure 9. Raw and statistical CHF data.

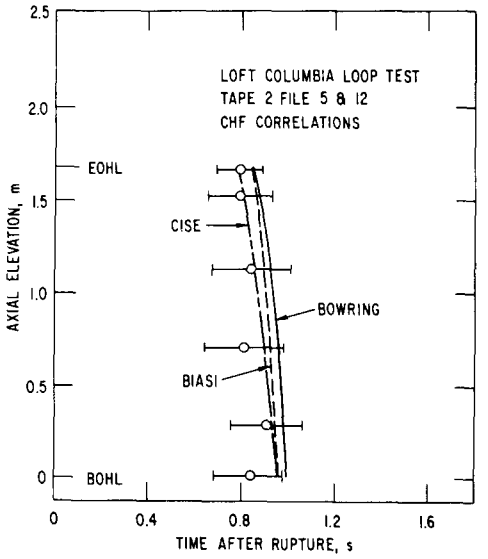

Figure 10. CHF predictions using round-tube correlations.

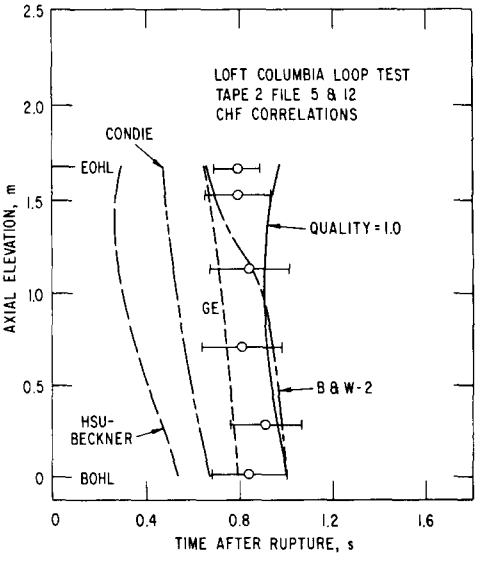

Figure 11. CHF predictions using rod-bundle correlations.

test was conducted with four central high-power rods. During blowdown the power to the 40-rod bundle was automatically decayed to simulate fuel-rod response. Core overheating was first detected at about 23.5 s when the core power had decayed to 6 per cent of its initial value. In spite of the nonuniform radial power, a core-average thermal-hydraulic calculation might be adequate to reveal the dryout characteristic. Furthermore, the dryout time did not exhibit any significant difference between the high- and low-power rods.

Mass flow rate at the core inlet was measured using the turbine meter, drag disk, and γ densitometer. Two independent mass-flow-rate measurements are shown in figures 15 and 16. Between 20 and 30 s, which is the period of interest here, the two measurements exhibited some discrepancies. This may be inevitable because at such low mass flow and high void fraction mass-flow measurements are extremely difficult. In view of the measurement uncertainty, both mass-flow measurements were used in two separate CODA calculations.

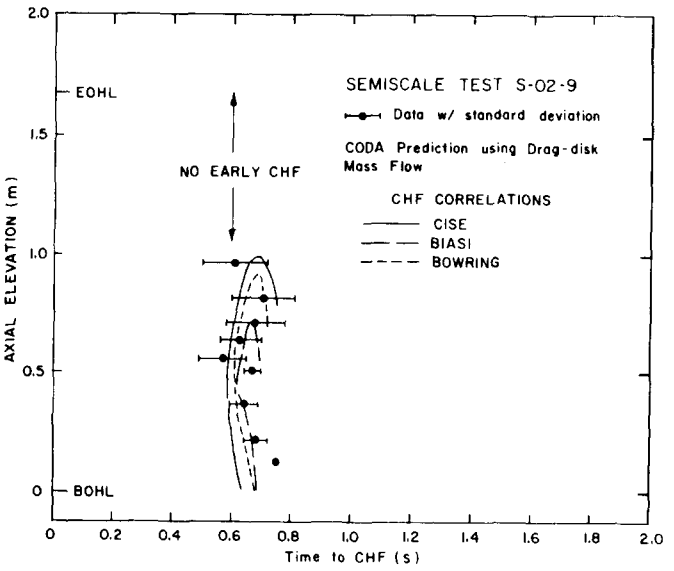

Figure 12. CHF predictions using round-tube correlations.

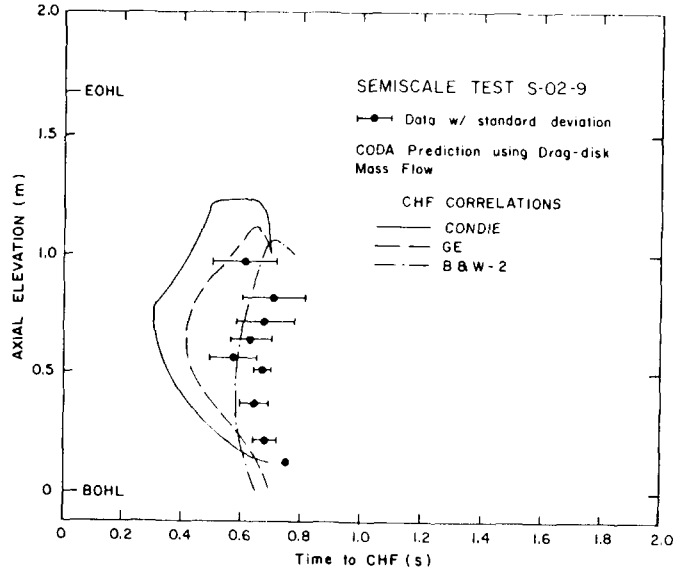

Figure 13. CHF predictions using rod-bundle correlations.

In this test, the round-tube and rod-bundle correlations failed to predict the onset of CHF. Only the Griffith–Zuber and Hsu–Beckner correlations predict CHF as shown in figure 17 and 18 respectively. Figure 17 shows that the dryout times can be bracketed by the two cases studied using the Griffith–Zuber correlation. This is a surprisingly good result in view of the fact that large uncertainties are involved in the mass-flow boundary condition. The calculated local mass velocity at CHF was about 100 kg/m^{2}s. The Hsu–Beckner correlation on the other hand, underestimated the dryout times for the top half of the core. In fact, it predicted dryout to occur first at the top of the core in contradiction with the data.

Semiscale Mod–3 blowdown tests. Semiscale Tests S–07–3 and S–07–9 were conducted in the Mod–3 system with a full-length 5×5 PWR bundle and with similar initial hydraulic conditions. For Test S–07–9 the nine central rods were powered 12.8 per cent higher than the remaining 14 rods. In addition, considerably improved in-core instrumentation was reported for this test. As far as the core thermal response is concerned, no significant difference was observed in the CHF behavior. CHF was first measured in the peak heat-flux zone at about 0.6 s

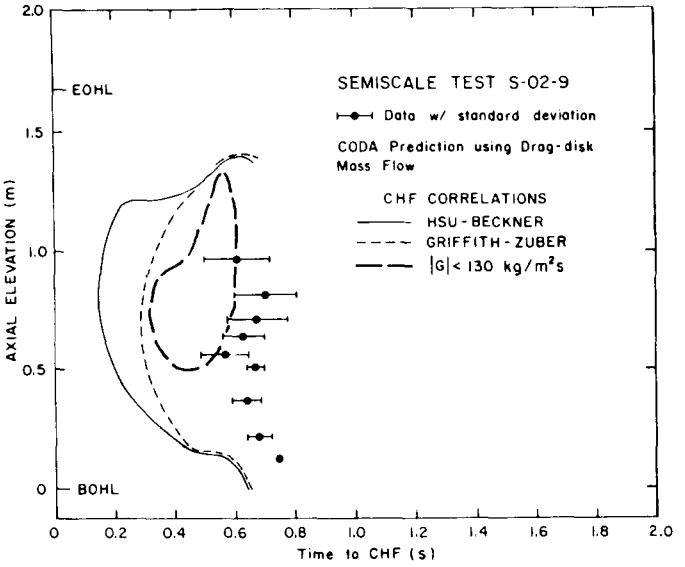

Figure 14. CHF predictions using Hsu–Beckner and Griffith–Zuber correlations.

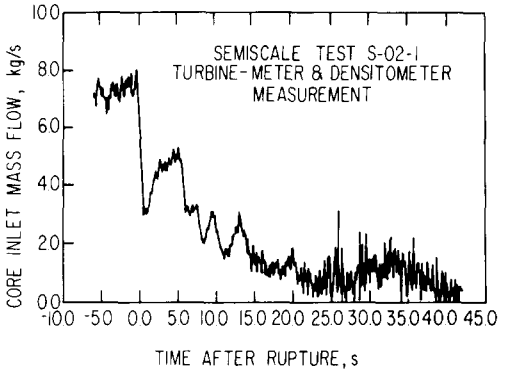

Figure 15. Core inlet mass flow based on turbine meter.

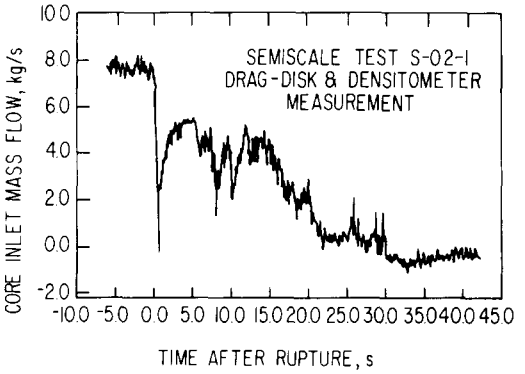

Figure 16. Core inlet mass flow based on drag disk.

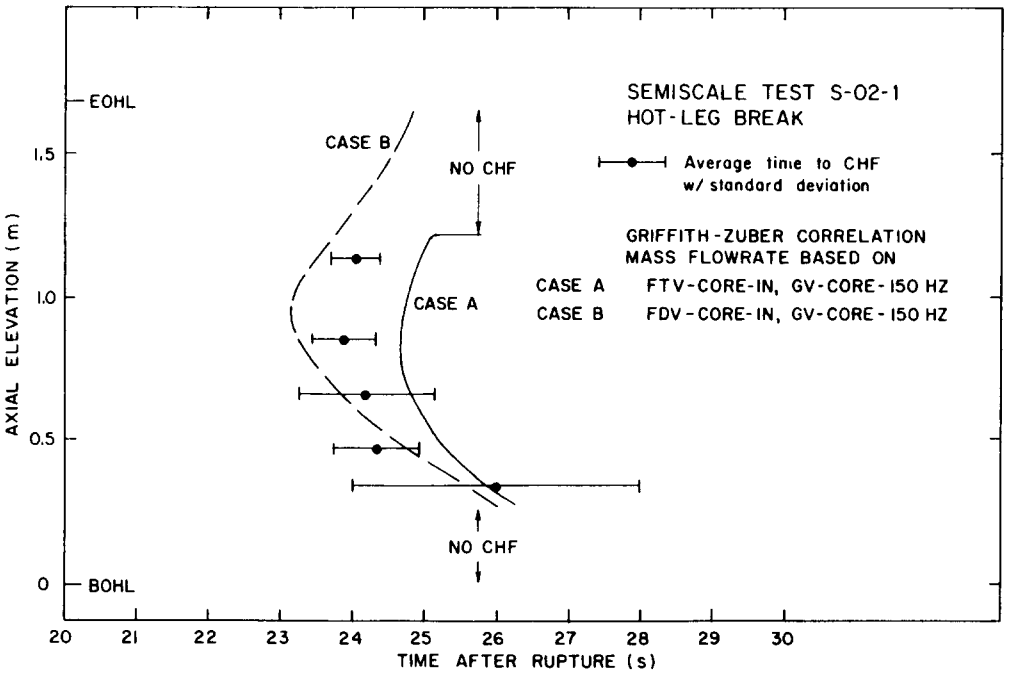

Figure 17. CHF predictions using Griffith–Zuber correlation.

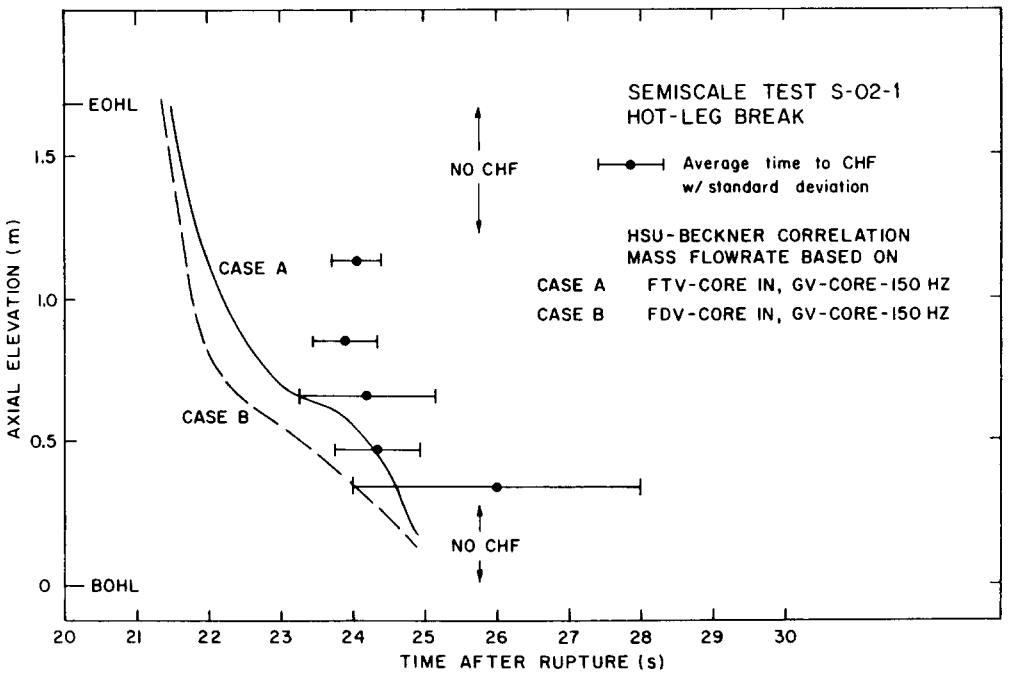

Figure 18. CHF predictions using Hsu–Beckner correlation.

while the lowest region experienced overheating after 1.0 s. In figure 19, the round-tube correlations predicted the CHF in the middle and upper portions of the core well but underpredicted the time somewhat in the bottom region. GE correlation yielded similar results with the exception that it predicted CHF at the upper most region also as shown in figure 20. B&W-2 correlation failed to predict the data trend while Condie correlation underpredicted the time in general. Both Hsu–Beckner and Griffith–Zuber correlations predicted CHF too early as shown in figure 21.

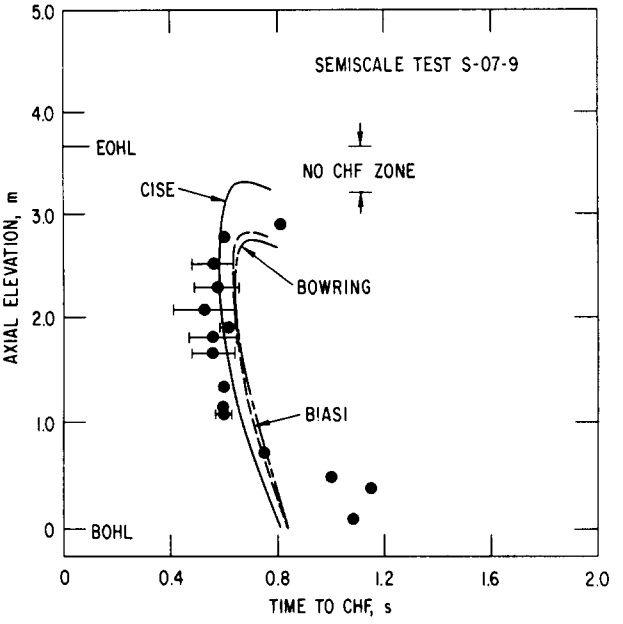

Figure 19. CHF predictions using round-tube correlations.

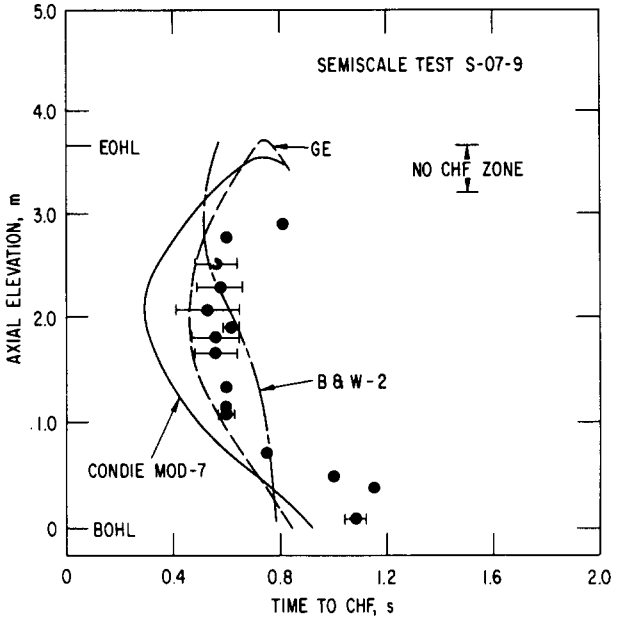

Figure 20. CHF predictions using rod-bundle correlations.

PBF blowdown test. PBF LOCA test series consists of three actual nuclear-fuel blowdown tests with Test LOC-11C being conducted at the highest power. The core consists of four separately shrouded fuel rods which are of typical PWR design except for an active length of 0.91 m. An understanding of the fuel-rod steady-state behavior is necessary in order to define the initial state and characteristics of the fuel rod. Figure 22 shows the capability of HETRAP in predicting the centerline temperature while the fuel rods were brought up to steady-state power in Test LOC-11C. The fuel centerline temperature is closely related to the initial stored energy which primarily governs the clad-temperature rise in post-CHF period. During blowdown the cladding surface closely followed the system saturation temperature prior to any onset of CHF. The surface heat flux is no longer a strong function of the assumed heat-transfer

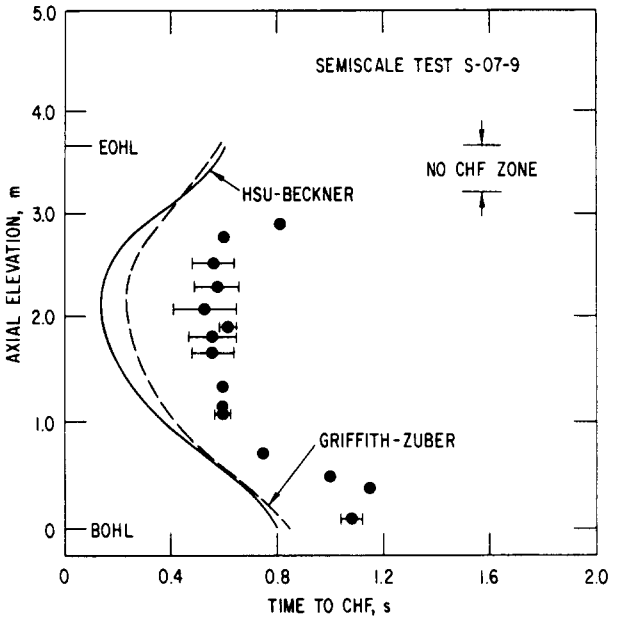

Figure 21. CHF predictions using Hsu–Beckner and Griffith–Zuber correlations.

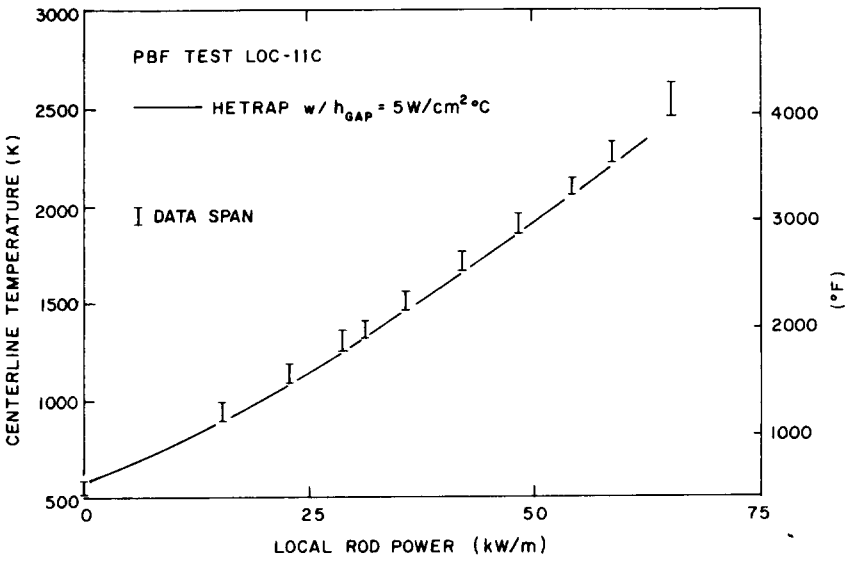

Figure 22. Prediction of centerline temperature as a function of local rod power.

coefficient because the heat-transport process is primarily rate-limited inside the fuel rod and at the gap interface. To a good approximation, the surface heat flux during blowdown can be represented by the curve shown in figure 23.

During the transient both the cladding thermocouple and the elongation transducer simultaneously detected a rapid rise at the peak-power elevation at 1.6 s. CHF predictions are shown in figure 24. Once again, none of the round-tube correlations predicted CHF. At the measured CHF onset, the local mass velocity was estimated to be 27 kg/m^2·s, at nearly stagnation condition. The Condie correlation yielded the closest t_{CHF}, while GE and Griffith–Zuber correlations are considered acceptable. The Hsu–Beckner correlation is unacceptable, as it underestimated the time considerably.

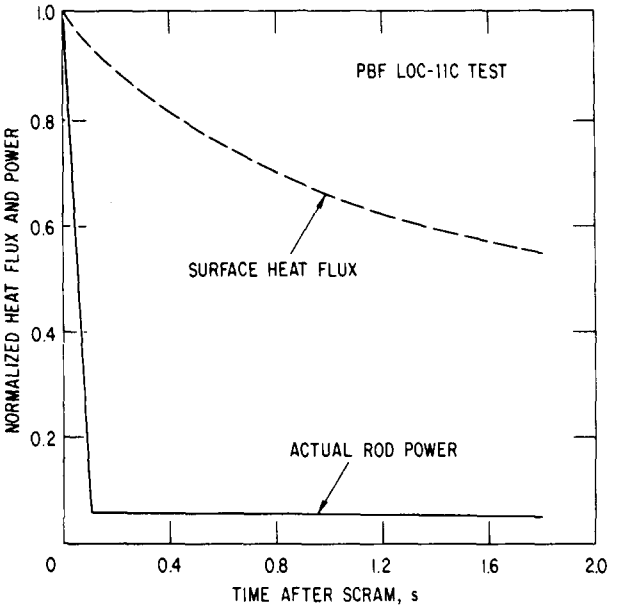

Figure 23. Estimated surface heat flux during blowdown.

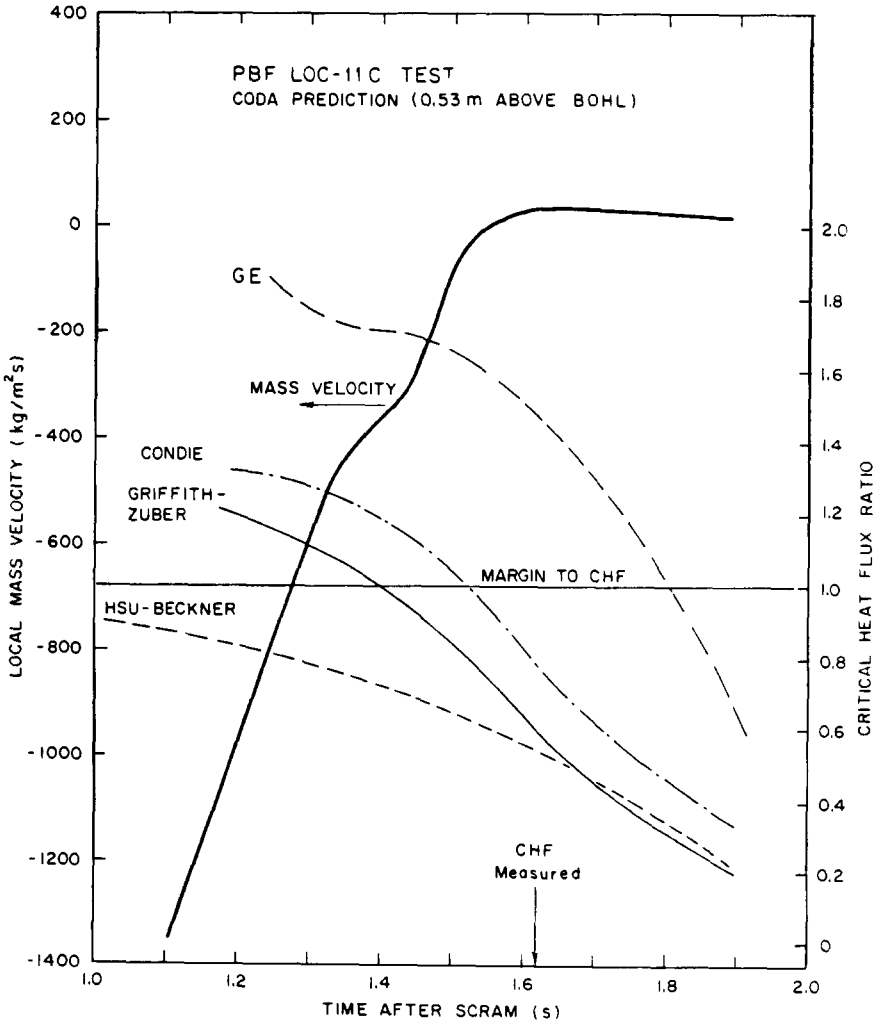

Figure 24. CHF prediction results.

4.3 *Comments on CHF correlations and phenomenon*

Table 3 summarizes the prediction results for the blowdown experiments. Obviously no one single correlation exhibits good prediction for all the data. In CE/EPRI Test BHT-25, no CHF was measured during blowdown, and indeed none of the correlations predicted CHF; therefore, they all received the same score in table 3. Most of the blowdown test exhibited early CHF ($t_{CHF} \simeq 1$ s) which occurred entirely in inlet break situations with rapid flow reversal in the heated core. It is important to note also that CHF did not occur during the flow reversal period but rather after flow had reestablished itself in the downward direction.

In general, the early CHF were best predicted by the round-tube correlations which are applicable over a wide range of pressures. In addition, the CISE (round-tube) correlation has been shown by Leung (1980) to correlate some limited steady-state rod-bundle CHF data as well. One such prediction is shown in figure 25. For the B&W 9-rod bundle (1969) with axially and radially uniform power, the heated-equivalent diameters for various subchannels are rather uniform, and in essence the cross-sectional average mass velocity and quality were used in the prediction. The agreement is encouraging in comparison with the well-known B&W-2 rod-bundle correlation which was proposed to correlate only a limited amount of these data (within $P > 13.8$ MPa, $G > 1000$ kg/m^2·s, and $x < 0.20$).

As pointed out by Bjornard & Griffith (1977), the local quality is increasing rapidly at the onset of the early CHF, and hence a wide range of CHF conditions is being swept through in a very short time. In such circumstances, an appreciable error in the prediction of the magnitude of CHF may-result in only an insignificant error in the predicted t_{CHF}. This may indeed help to explain the degree of success obtained with the round-tube correlations. However, it is worth noting also that an accurate prediction of the CHF value is essential in accurately delineating the CHF region from the non-CHF region.

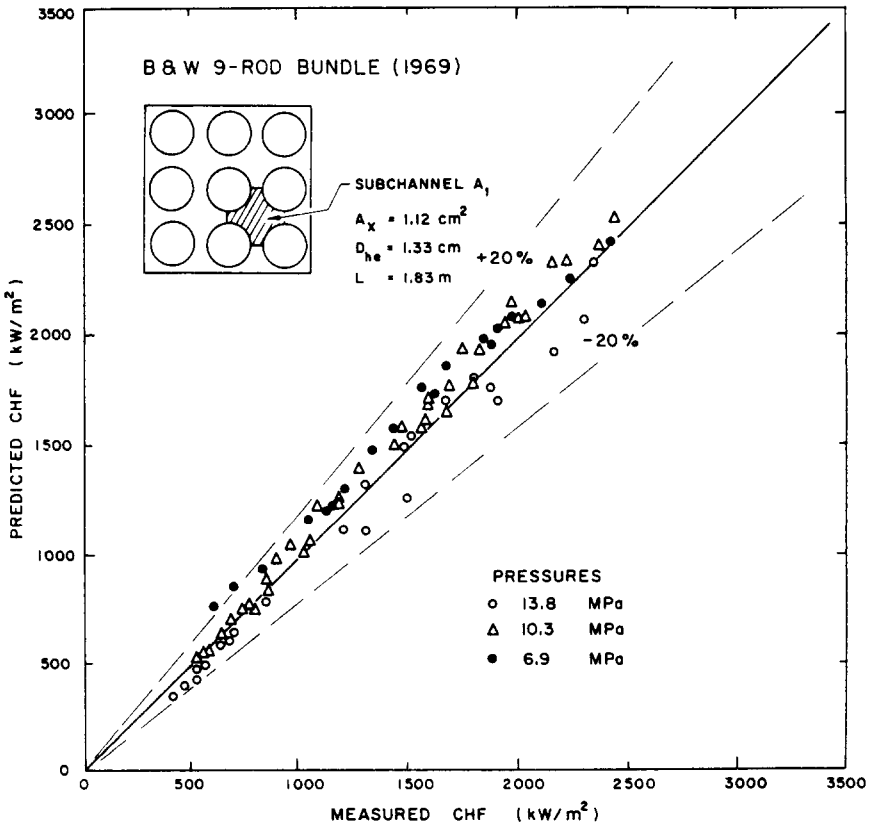

Figure 25. Prediction of B&W CHF data by CISE correlation.

Table 3. Summary of blowdown heat transfer results

Tests and Specifications	Bowring	Biasi	CISE	Griffith -Zuber	GE	Condie Mod-7	B&W-2	Hsu-Beckner	x = 1.0
CE/EPRI Rod-bundle BHT-25	○	○	○	○	○	○	○	○	○
LOFT Columbia loop	○	○	○	●	○	o	○	●	○
PBF LOC-11C	●	●	●	○	○	○	●	●	●
THTF Bundle #1									
Test 105	o	○	○	o	○	o	o	●	○
Test 104	○	○	○	o	○	o	o	●	○
Test 178	○	○	○	o	o	o	o	o	○
Test 181	o	○	○	o	o	o	●	o	○
Test 177	●	○	○	○	○	o	●	o	○
Semiscale Mod-1									
S-02-1	●	●	●	○	●	●	●	o	●
S-02-9	o	○	○	●	o	o	○	●	●
S-29-2	○	o	○	●	o	o	o	●	●
S-28-1 (early and delay CHF)	○●	○o	○o	●○	○○	o●	○o	o●	●●
S-06-6	●	●	●	○	●	○	●	o	●
Semiscale Mod-3									
S-07-3	○	○	○	●	○	o	○	●	o
S-07-9	○	○	○	●	o	o	o	●	o

Notation: ○ Good prediction; o Acceptable (usually early T_{CHF} predicted; ● Unacceptable (many cases no CHF prediction)

As for the rod-bundle correlations, they appear to perform less satisfactory. Most of the available rod-bundle data (including both low and high quality CHF) were used to obtain the Condie correlation, and it is not clear why it performed so marginally for the blowdown data. As a whole, it tends to correlate the delay CHF much better than the early ones. The GE correlation, on the other hand, performed adequately for most of the early CHF data, but was found incapable in the prediction of delay CHF in the Semiscale data. The B&W-2 correlation did not work well under blowdown conditions which in most cases were outside its applicable ranges.

The Hsu–Beckner correlation was derived empirically with some early blowdown data, but in the present study this correlation was found inadequate and sometimes yielded very conservative predictions.

The Griffith–Zuber correlation cannot be used without some low-flow criteria. Indeed the correlation itself is a modified form of the maximum pool boiling heat flux formula and was obtained at very low upflow and sometimes counter-current flow conditions. Bjornard and Griffith recommended its use for the following mass velocity,

$$-667 < G < 100\ \text{kg/m}^2\text{·s}\,.$$

In the present study, this correlation was found to predict all the delay CHF very well. Based on the limited amount of data, it is tentatively recommended for the following range,

$$-240 < G < 100\ \text{kg/m}^2\text{·s}\,.$$

This criterion is strongly affected by the reported mass flow measurement, and mass velocity of this low magnitude is difficult to measure accurately in these experiments. The success of this correlation in a downflow situation is illustrated in figure 26 where the Semiscale Test S–06–6 results are compared with the Griffith–Zuber correlation. The prediction is seen to be rather conservative without imposing a mass-velocity criterion. Constant mass-velocity curves of -200 and $-270\ \text{kg/m}^2\text{·s}$ were drawn in the figure, and they were seen to correlate the low-power and high-power rod data reasonably well respectively. Once again, these mass

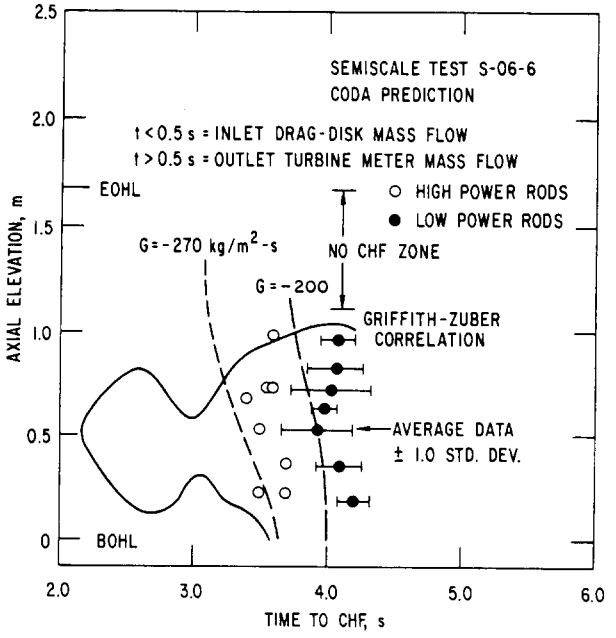

Figure 26. CHF prediction using Griffith–Zuber correlation.

velocity values are suggested here in lieu of extensive comparisons to data. In fact, such data (delay CHF) are rather limited at this time.

In general, the delay CHF occurred in a quiescent state, at low and slowly decaying mass flow rate. One reason the round-tube correlations all failed in predicting this long-term CHF is simply that it occurred at the very low end of the applicable velocity range. The early CHF, on the contrary, occurred at much higher but rapidly decaying mass velocity. In many instances, the early CHF can be well correlated by the $x = 1.0$ criterion, and this is certainly indicative of an annular-flow dryout-type phenomenon. On the other hand, the success of the Griffith–Zuber correlation in predicting delay CHF suggested a pool-boiling-type hydrodynamic crisis.

Finally, it should be pointed out about the limitation of present CHF correlations in small-break LOCA analysis such as the one that occurred at Three Mile Island Unit 2. During this particular accident the core overheating occurred at about 110 min at less than 1 per cent decay power. The overheating was brought about as the two-phase mixture level receded, thus uncovering and exposing the upper portion of the core to a nearly stagnant steam environment. At such low heat-flux conditions, the applicability of the present CHF correlations would be highly questionable. Indeed, under such accident conditions, the hydrodynamic of the boil-up core has been demonstrated experimentally by Ogaswara *et al.* (1973) to play a major role in determining the coolability of the fuel cladding.

5. CONCLUSIONS AND RECOMMENDATIONS

Extensive blowdown heat-transfer data have been examined using a simple one-dimensional thermal-hydraulic code. Transient CHF predictions were obtained entirely on the basis of local conditions. Hence, reliable local fluid conditions calculation is essential and this depends not only on the two-phase flow formulation but also on the boundary condition input such as inlet mass flowrate. Many of the thermal-hydraulic calculations performed by the code have demonstrated good agreement with in-core data, although much of the discrepancy can be reduced with improved two-phase flow instrumentation and in-core measurements.

Based on thorough analyses of the rod-bundle blowdown data, the following recommendation is made for transient CHF prediction. In general, the local condition approach appears to be adequate. The early CHF ($t_{CHF} \sim 1.0$ s) that occurred after flow reversal in these experiments was best predicted by the CISE and Biasi correlations. These two round-tube correlations are simple to use and have a wide range of applicability. Furthermore, the CISE correlation has been demonstrated to correlate steady-state rod-bundle CHF data as well. However, these round-tube correlations failed to predict delay CHF which occurred in a quiescent state with slowly decaying mass flow. The Griffith–Zuber low-flow correlation correlated the delay CHF well and it is recommended for the following mass velocity,

$$-240 < G < 100 \text{ kg/m}^2\cdot\text{s}.$$

In some cases, the $x = 1.0$ criterion matches the early CHF data well, and this is certainly indicative of an annular-flow dryout phenomenon. As for the delay CHF, a pool-boiling-type hydrodynamic crisis is suggested.

Acknowledgements—We wish to thank the U.S. Nuclear Regulatory Commission for supporting this work, and to acknowledge many helpful discussions with Y. Y. Hsu (NRC), L. B. Thompson (NRC), D. M. Snider (EG&G) and W. G. Craddick (ORNL).

BERTOLETTI, S. *et al.* 1965 Heat transfer crisis with steam–water mixtures. *Energia Nucl.* **12**, 121–172.

BIASI, L. *et al.* 1967 Studies on burnout—3. *Energia Nucl.* **14**, 530–536.

BJORNARD, T. A. & GRIFFITH, P. 1978 PWR blowdown heat transfer. *Symp. Thermal and Hydraulic Aspects of Nuclear Reactor Safety, Vol.* 1, *Light Water Reactors*, pp. 17–41.

BOWRING, R. W. 1972 A simple but accurate round tube, uniform heat flux dryout correlation over the pressure range 0.7–17 MN/m^2. AEEW-R789.

BUCKLAND, R. J., COPPIN, C. E. & WHITE, C. E. 1978 Experiment data report for PBF-LOCA Tests LOC-11B and 11C. NUREG/CR-0303, also EG&G Rep. TREE-1232.

CLEMONS, V. D. *et al.* 1977 PWR blowdown heat transfer separate-effects program—thermal-hydraulic test facility experimental data report for Test 105. ORNL/NUREG/TM-143.

COLLINS, B. L., COPPIN, C. E. & SACKETT, K. E. 1977 Experiment data report for Semiscale Mod-1 Test S-28-1 (Steam Generator Tube Rupture Test). EG&G Rep. TREE-NUREG-1148.

CONDIE, K. G. *et al.* 1978 Development of the MOD7 CHF Correlation. EG&G Rep. PN-181-78.

CRADDICK, W. G. *et al.* 1979 Quick look report on thermal hydraulic test facility Test 178. ORNL/BDHT-2250.

CRADDICK, W. G. *et al.* 1979 Quick look report on thermal hydraulic test facility Test 181. ORNL/BDHT-2254.

CRADDICK, W. G. *et al.* 1980 PWR blowdown heat transfer separate-effects program—thermal hydraulic test facility experimental data report for Test 177. ORNL/NUREG/TM-295.

CRAPO, H. S., JENSEN, M. F. & SACKETT, K. E. 1975 Experimental data report for Semiscale Mod-1 Test S-02-1 (Blowdown Heat Transfer Test). ANCR-1231.

CRAPO, H. S., JENSEN, M. F. & SACKETT, K. E. 1976 Experiment data report for Semiscale Mod-1 Tests S-02-9 and S-02-9A (Blowdown Heat Transfer Tests). ANCR-1236.

CRAPO, H. S. & SACKETT, K. E. 1976 Experiment data report for Semiscale Mod-1 Test S-29-2 (Integral Test from Reduced Pressure). ANCR-NUREG-1328.

DAVIS, C. B. 1978 Assessment of the RELAP/MOD6 thermal-hydraulic transient code for PWR experimental applications— 1. Assessment analysis. EG&G Rep. CAAP-TR-78-035.

ESPARZA, V. & SACKETT, K. E. 1977 Experiment data report for Semiscale Mod-1 Test S-06-6 (LOFT Counterpart Test). EG&G Rep. TREE-NUREG-1126.

GELLERSTEDT, J. S. *et al.* 1969 Correlation of critical heat flux in a bundle cooled by pressurized water. Presented at ASME Winter meeting., Los Angeles.

GILLINS, R. L. *et al.* 1978 Experiment data report for Semiscale Mod-3 blowdown heat transfer Test S-07-3 (Baseline Test Series). NUREG/CR-0356.

GOTTULA, R. C. 1978 LOFT transient (blowdown) critical heat flux tests. EG&G Rep. TREE-NUREG-1240.

GRIFFITH, P. PEARSON, J. F. &LEPKOWSKI, R. J. 1977 Critical heat flux during a loss-of-coolant accident. *Nucl. Safety* **18**, 298–305.

HSIA, A. H *et al.* 1977 Rod bundle blowdown heat transfer tests simultating pressurized water reactor loss of coolant accident conditions. EPRI NP-113.

HSU, Y. Y. & BECKNER, W. D. 1977 A correlation for the onset of transient CHF. Unpublished report, as cited by L. S. Tong and G. L. Bennett 1977 NRC water-reactor safety-research program. *Nucl. Safety* **18**, 1–40.

LEUNG, J. C. M. 1978 Critical heat flux under transient conditions, literature survey. ANL-78-39 (NUREG/CR-0056).

LEUNG, J. C. M. & GALLIVAN, K. A. 1980 Prediction of critical heat flux during transients. ANS *Thermal Reactor Safety meeting*, Knoxville, April. CONF-800403 **2**, pp. 1229–1239.

LEUNG, J. C. M. 1980 Transient critical heat flux and blowdown heat transfer studies. Ph.D. Thesis, Northwestern University, also ANL-80-53 (NUREG/CR1559).

MALANG, S. 1974 HETRAP: A heat transfer analysis program. ORNL-TM-4555.

MEYERS, J. E. 1961 Hydrodynamic models for the treatment of reactor thermal transients. *Nucl. Sci. Engng* **10**, 269–277.

MIYASAKI, D. H. *et al.* 1979 Experimental data report for Semiscale Mod-3 blowdown heat transfer Test S-07-9 (Baseline Test Series). NUREG/CR-0815.

OGASWARA, H. *et al.* 1973 Cooling mechanism of low pressure coolant injection system of boiling water reactors and other studies on the loss-of-coolant accident phenomena. *ANS Topical meeting on Water Reactor Safety*, Salt Lake City, March. CONF-730304, pp. 351–370.

SILVERMAN, S. 1977 Principles of operation and data reduction techniques for the LOFT drag disc turbine transducer. EG&G Rep. TREE-NUREG-1109.

SLIFER, B. C. 1971 Loss-of-coolant accident and emergency core cooling models for General *Electric boiling water reactors. GE Rep. NEDO*-10329.

SNIDER, D. M. 1977 Analysis of the thermal-hydraulic behavior resulting in early critical heat flux and evaluation of CHF correlations for the Semiscale core. EG&G Rep. TREE-NUREG-1073.

TRAC-P1A, 1979 An advanced best estimate computer program for PWR LOCA analysis. NUREG/CRO665, LA-7777-MS.

TONG, LS S. 1967 Prediction of departure from nucleate boiling for an axilly non-uniform heat flux distribution. *J. Nucl. Energy* **6**, 241–248.

APPENDIX

The equations of CHF correlations used in the present study are described here. No distinction is made between upflow and downflow, and therefore the abolute value mass velocity ($|G|$) is to be used in these correlations. The following SI units are to be used: ϕ_{CHF} = critical heat flux, kW/m^2; G = mass velocity, kg/m^{2}s; D = heated equivalent diameter, m; h_{LG} = heat of vaporization, kJ/kg; P = pressure, MPa (MN/m^2); and x = quality.

(1) *Bowring correlation*

$$\phi_{CHF} = \frac{GDh_{LG}}{4C}(A - x)$$

with $A = 2.317\ F_1/(1 + 0.0143\ F_2 D^{0.5}\ G)$, $C = 0.077\ F_3\ DG/[1 + 0.347\ F_4\ (G/1356)^n]$.

The parameters F_1, F_2, F_3 and F_4 are functions of the normalized pressure P_R,

$$P_R = 0.145\ P.$$

For $P_R \leq 1$

$$F_1 = P_R^{18.942}\{\exp[20.89\,(1 - P_R)] + 0.917\}/1.917,$$

$$F_2 = 1.309\ F_1/\{P_R^{1.316} \exp[2.444\,(1 - P_R)] + 0.309\},$$

$$F_3 = \{P_R^{17.023} \exp[16.658(1 - P_R)] + 0.667\}/1.667,$$

and

$$F_4 = F_3 P_R^{1.649}.$$

For $P_R > 1$

$$F_1 = P_R^{-0.368} \exp[0.648(1 - P_R)],$$

$$F_2 = F_1 P_R^{0.448}/\exp\,[0.245(1-P_R)]\,,$$

$$F_3 = P_R^{0.219}\,,$$

and

$$F_4 = F_3 P_R^{1.649}\,.$$

(2) *Biasi correlation*

CHF is given by the higher of the two values based on the following two equations;

$$\phi_{\mathrm{CHF}} = \frac{2.75\times 10^4}{(100\,D)^n\,G^{0.167}}\left(\frac{1.47\,F}{G^{0.167}} - x\right)$$

for low quality, and

$$\phi_{\mathrm{CHF}} = \frac{1.51\times 10^5\,H}{(100\,D)^n\,G^{0.6}}(1-x)$$

for high quality where

$$n = 0.4 \text{ for } D \geq 0.01\ m\,,$$

$$n = 0.6 \text{ for } D < 0.01\ m\,,$$

and

$$F = 0.7249 + 0.99\,P\exp\,(-0.32\,P),$$

$$H = -1.159 + 1.49\,P\exp\,(-0.19\,P) + \frac{8.99\,P}{1+10\,P^2}\,.$$

For values of G below 300 kg/m^{2}s the second equation for high quality is used.

(3) CISE correlation

$$\phi_{\mathrm{CHF}} = \frac{1.258\,h_{LG}}{D^{0.4}\left(\frac{1}{P_r}-1\right)^{0.4}}(a-x)$$

and

$$a = (1-P_r)/(G/1000)^{0.333}$$

where $P_r = P/P_c$ and $P_c = 22.1$ MPa, critical pressure.

(4) *B&W-2 correlation*

$$\phi_{\mathrm{CHF}} = \frac{(a-bD)[A_1(A_2G)^{A_3+A_4(P-13.8)} - A_9\,Gxh_{LG}]}{A_5(A_6G)^{A_7+A_8(P-13.8)}}$$

where $a = 3.644\times 10^{-3}$; $b = 5.059\times 10^{-2}$; $A_1 = 0.37\times 10^8$; $A_2 = 4.36\times 10^{-4}$; $A_3 = 0.83$; $A_4 = 0.1$; $A_5 = 12.71$; $A_6 = 2.25\times 10^{-3}$; $A_7 = 0.71$; and $A_8 = 3.0\times 10^{-2}$.

(5) *Condie correlation*

$$\phi_{\mathrm{CHF}} = 5.1 \times 10^3 \frac{(7.37 \times 10^{-4}\, G)^{[0.1775 \ln (1+x)]}}{(1+x)^{3.391}\, P^{0.323}\, RPF^{1.053}}$$

where RPF = radial power factor; set to 1.0 in present study.

(6) GE *correlation*

$$\phi_{\mathrm{CHF}} = 3.155 \times 10^3 (0.84 - x)$$

for $G < 680\ \mathrm{kg/m^2 s}$, and

$$\phi_{\mathrm{CHF}} = 3.155 \times 10^{-3} (0.80 - x)$$

for $G \geq 680\ \mathrm{kg/m^2 s}$.

(7) *Hsu–Beckner correlation*

$$\frac{\phi_{\mathrm{CHF}} - \phi_{\mathrm{steam}}}{\phi_{\substack{W-3 \\ x=0}} - \phi_{steam}} = [1.76(0.96 - \alpha)]^{1/2}$$

where α = bulk void fraction; $\phi_{\mathrm{steam}} = h_{D-B}(T_{\mathrm{wall}} - T_{\mathrm{sat}})$; h_{D-B} = Dittus–Boelter heat-transfer coefficient for steam, and

$$\phi_{\substack{W-3 \\ x=0}} = 3.01 \times 10^3 \{[1.04 + 1.09 \times 10^{-4} G][2.192 - 7.69 \times 10^{-2} P].$$

Since ϕ_{steam} is small, as compared to ϕ_{CHF} and $\phi_{\substack{W-3 \\ x=0}}$, it is ignored; hence

$$\phi_{\mathrm{CHF}} = \phi_{\substack{W-3 \\ x=0}} [1.76(0.96 - \alpha)]^{1/2}.$$

(8) *Griffith–Zuber correlation*

$$\phi_{\mathrm{CHF}} = (1 - \alpha) 0.131\, \rho_G\, h_{LG} \left[\frac{\sigma g (\rho_L - \rho_G)}{\rho_G^2}\right]^{1/4}$$

where g = gravitational constant, 9.8 m/s^2; σ = surface tension, N/m; ρ_g = vapor density, kg/m^3; and ρ_L = liquid density, kg/m^3.